

Enhanced Uranium Sorption on Aluminum Oxide Pretreated with Arsenate. Part II: Spectroscopic Studies

YUANZHI TANG,^{*,†} JASON MCDONALD,
AND RICHARD J. REEDER

Department of Geosciences and Center for Environmental
Molecular Science, State University of New York, Stony Brook,
New York 11794-2100

Received August 25, 2008. Revised manuscript received
March 10, 2009. Accepted April 14, 2009.

In a companion study, we demonstrated that pretreatment of γ -alumina surface with arsenate enhances uranyl uptake under acidic conditions, where uranyl otherwise sorbs poorly. Here, we examine the local structure and long-range order of the sorption products by using X-ray absorption spectroscopy (XAS) and X-ray diffraction (XRD). Arsenate was chosen for the pretreatment because of its high affinity for binding with uranyl and alumina, and because it is an analog for environmentally abundant and commercially accessible phosphate. It also facilitates characterization of sorption products using As K-edge XAS, which complements U L_{III} -edge XAS. Fitting results suggest the formation of U–As precipitates with structures similar to $UO_2HAsO_4 \cdot 4H_2O$ (trögerite) and likely U polymeric species at high U concentrations. The ratios among surface-sorbed uranyl, U–As precipitates, and uranyl polymeric species are dependent on the $[As]_{initial}/[U]_{initial}$ ratio and absolute initial U concentration. XRD suggests the precipitates are likely to be highly disordered and poorly crystalline. Current findings evaluate the mechanism by which the pretreatment results in enhanced U uptake and stability and provides a conceptual basis for designing other pretreatment technologies for uranium remediation.

1. Introduction

Uranium is an environmental pollutant associated with milling, mining, isotopic enrichment activities, and nuclear waste storage at U.S. Department of Energy sites and elsewhere. It is considered a hazard because of its radioactivity as well as toxicity as a heavy metal. Many field demonstrations and laboratory studies have evaluated uranium retardation and remediation by different techniques, including in situ reduction, precipitation, sorption, and installation of permeable reactive barriers (1–4). Under oxidizing environments, U(VI) is the stable oxidation state, existing almost exclusively as uranyl UO_2^{2+} , and is much more soluble and mobile than the other common oxidation state U(IV). Inasmuch as sorption onto a mineral surface is one of the most important means of retarding uranyl mobility in the natural environment (1), suitable sorbents should have a strong affinity for uranyl sorption or act as a reductant

to reduce U(VI) to U(IV) (4). The long-term effectiveness of such sorbents also depends strongly on their surface properties and the final state of the retained uranium. Because of the low solubility of uranyl phosphate compounds in geological settings (5), phosphate-containing materials have been tested at several demonstration sites (4, 6). At most of the studied sites, decreases of total dissolved uranium concentration in the groundwater were observed. However, detailed characterization of the sorption products (i.e., their chemical speciation) is critical for understanding their long-term stability and potential for remobilization. Fuller et al. (6) studied the sorption products from a demonstration site, which uses a biogenic phosphate material (apatite-containing bone charcoal) and found that under existing groundwater conditions the immobilized uranium existed mostly as surface complex(es), which may be more susceptible to remobilization than precipitated solids. A molecular scale understanding of sorption products also provides the basis for improving sequestration technologies.

In a companion paper (7), we explored the batch uptake behavior of uranyl by γ -alumina surfaces that were pretreated with an inorganic ligand having a high affinity for both uranyl and the solid surface. Arsenate was used as an analog of phosphate because it allows for more convenient characterization of the sorption products by X-ray absorption spectroscopy (XAS). Our observations showed greatly enhanced uranyl sorption on the pretreated surface at acidic pH values. This possibly suggests that arsenate-pretreated surfaces, and by analogy phosphate-pretreated surfaces, favor uranyl complexation and precipitation. The effects of alumina loading, initial arsenate concentration for pretreatment, and uranyl concentration were examined. Desorption experiments also indicated enhanced stability of uranyl on pretreated surfaces, suggesting less susceptibility to remobilization. In this study, we examine the local structure and long-range order of the final sorption products of uranyl reacted with arsenate-pretreated alumina by combining U L_{III} - and As K-edge XAS and X-ray diffraction.

2. Materials and Methods

2.1. Batch Sorption Experiments. Details of batch sorption procedures have been described in detail by Tang and Reeder (7). The pretreatment (prt) process involved reacting arsenate with aged alumina suspensions for 24 h, followed by the addition of uranyl. Uranyl sorption samples on arsenate-pretreated alumina are labeled as prt–alumina loading (g/L)– $[As]_{ini}$ (mM)– $[U]_{ini}$ (mM). All sorption products were centrifuged, and the wet paste was mounted for XAS analysis. Portions of the wet pastes were dried under N_2 atmosphere and ground for XRD analysis.

Two primary series of sorption samples were chosen for XAS analysis: (1) a low concentration group, with alumina loading of 2 g/L, $[As]_{ini}$ 0.05–1 mM, and $[U]_{ini}$ 0.05–0.8 mM, and (2) a high concentration group, with alumina loading of 10 g/L, $[As]_{ini}$ 2 mM, and $[U]_{ini}$ 1–4 mM. Previous studies show that uranyl can form polymeric species and precipitates at relatively high concentrations (8–11); therefore, comparisons between the two concentration groups allow us to examine the effect of absolute $[U]_{ini}$ on the final sorption products. Spectra were also collected on two U (or As) sorption samples on untreated alumina at pH 4 ± 0.2 . They are labeled as U (or As)–alumina loading (g/L)– $[U]_{ini}$ (or $[As]_{ini}$) (mM). Information for all sorption samples examined by XAS is given in Table 1.

2.2. Model Compounds. Three uranyl arsenate compounds were synthesized and used as model structures for XAS analysis, including $UO_2HAsO_4 \cdot 4H_2O$ (trögerite), UO_2 –

* Corresponding author phone: 617-496-3559; fax: 617-496-1023; e-mail: ytang@seas.harvard.edu.

† Current address: School of Engineering and Applied Science, Harvard University, 40 Oxford St., Cambridge, Massachusetts 02138.

TABLE 1. Information for EXAFS Samples

samples	[γ -Al ₂ O ₃] (g/L)	[As] _{ini} (mM)	[U] _{ini} (mM)	after U sorption			
				prt-As uptake ^a (%)	U uptake (%)	[U] _{solid} (μ mol/g)	[As] _{solid} (μ mol/g)
As-2-0.4	2	0.4	—	98.5	—	—	197.00
U-2-0.1	2	—	0.1	—	22.5	11.25	—
prt-2-0.05-0.05	2	0.05	0.05	97.3	24.3	6.08	24.75
prt-2-0.1-0.1	2	0.1	0.1	98.7	35.9	17.96	49.34
prt-2-0.4-0.1	2	0.4	0.1	99.7	69.4	34.68	199.34
prt-2-0.4-0.2	2	0.4	0.2	99.7	57.5	57.55	188.50
prt-2-0.4-0.4	2	0.4	0.4	99.7	48.6	97.08	190.86
prt-2-0.4-0.8	2	0.4	0.8	99.7	44.0	176.06	187.20
prt-2-1-0.1	2	1	0.1	65.2	96.1	48.06	357.20
prt-10-2-1	10	2	1	96.9	72.0	71.99	199.00
prt-10-2-2	10	2	2	96.9	52.7	105.48	198.68
prt-10-2-4	10	2	4	96.9	41.8	167.29	198.48

^a Arsenic percent uptake after the pretreatment process.

(H₂AsO₄)₂·H₂O, and (UO₂)₃(AsO₄)₂·5H₂O. Their structure types represent sheets, chains, and frameworks, with typical U:As (or P) ratios of 1:1, 1:2 and 3:2, respectively (12). Meta-schoepite, (UO₂)₄O(OH)₆·5H₂O, was also synthesized and used as a model compound to represent the extremely complex uranyl polymeric species or oxyhydroxide. Synthesis methods for all model compounds are described in the Supporting Information, and their structures are discussed later.

2.3. Synchrotron X-ray Absorption Spectroscopy Analysis. Details of X-ray absorption spectroscopy data collection and analysis are described in the Supporting Information. Errors for the fitting parameters are estimated from fits of model compounds. Estimated errors are ± 0.01 Å for the *R* value of the first oxygen shell and ± 0.05 Å for higher distance shells. For coordination numbers (CN), which are correlated to the Debye–Waller factor, the estimated errors are $\pm 20\%$ for the first oxygen shell and $\pm 40\%$ for shells at higher distances. Estimated errors for the Debye–Waller factors are ± 0.001 Å² for the first shell and ± 0.005 Å² for higher shells.

3. Results and Discussion

3.1. Aqueous Speciation. Aqueous speciation of uranyl at experimental conditions was calculated using the program PHREEQC (13) with the LLNL database provided with the program. Details are presented in the companion paper (7), where speciation calculations using phosphate as an analog for arsenate show strong complexation between uranyl and phosphate. (UO₂)₃(PO₄)₂·4H₂O and uranyl hydrogen phosphates with different hydration states were also shown to be oversaturated (7). Sandino and Bruno (14) studied the solution chemistry of (UO₂)₃(PO₄)₂·4H₂O and proposed that it may be the solubility-limiting phase in oxalic phosphate-containing systems at neutral to slightly alkaline pH. However, to our knowledge, neither (UO₂)₃(PO₄)₂·4H₂O nor its structural analog, (UO₂)₃(AsO₄)₂·4H₂O, has been reported to occur naturally. In fact, their synthesis involves recrystallization of the precursor phase chemnikovite, UO₂HPO₄·4H₂O (15), or trögerite, UO₂HAsO₄·4H₂O.

3.2. Structure of Model Compounds. U L_{III}-edge EXAFS data for the model compounds UO₂HAsO₄·4H₂O, UO₂·(H₂AsO₄)₂·H₂O, (UO₂)₃(AsO₄)₂·5H₂O, meta-schoepite, and U sorption sample (U-2-0.1) are shown in Figure 1, and their shell-by-shell fitting results are listed in Table SI-S1 of the Supporting Information. In all cases, the Fourier transforms are dominated by peaks at ~ 1 –2 Å in *R* space (not corrected for phase shift). The first peak centered at ~ 1.4 Å (1.8 Å in real space) is typical of compounds containing the uranyl moiety due to the strong backscattering of two axial oxygen atoms. The second strong peak centered at ~ 1.8 Å in *R* space

(except meta-schoepite) is due to the backscattering from equatorial oxygen atoms distributed at 2.29–2.47 Å. The reasons that meta-schoepite only shows subtle features at this position are discussed later.

The broad peak at 3–4 Å in the Fourier transforms of UO₂HAsO₄·4H₂O and UO₂(H₂AsO₄)₂·H₂O as seen in Figure 1b is due to the U–O_{ax}–U–O_{ax} multiple scattering (MS) contribution and backscattering from 4 As atoms at ~ 3.7 Å. The latter contribution results from uranyl bipyramids in the structural units of both compounds, where they share the corners with four arsenate tetrahedra. However, these two compounds have very different structures. UO₂HAsO₄·4H₂O has a space group of *P4/ncc* and belongs to the autunite–meta-autunite group with a U:As (or P) ratio of 1:1. It is isostructural with its phosphate analog chemnikovite, UO₂HPO₄·4H₂O, with a layered structure consisting of corrugated autunite-type sheets, connected by sharing vertices between uranyl square bipyramids and arsenate tetrahedra (Figure SI-S2 of the Supporting Information) (12, 16). Each uranyl bipyramide shares corners with four arsenate tetrahedra, and vice versa. UO₂(H₂AsO₄)₂·H₂O belongs to the less common walpurgite group with a U:P (or As) ratio of 1:2. It is not known to occur naturally. Its structure (space group *C2/c*) is based on infinite chains of uranyl pentagonal bipyramids (four connected within the chain, linked to arsenate tetrahedra. Each uranyl pentagonal bipyramide shares corners with four arsenate tetrahedra within the chain, whereas each arsenate tetrahedra only shares corners with two uranyl pentagonal bipyramids within the chain (17, 18).

(UO₂)₃(AsO₄)₂·5H₂O represents the less common phosphuranylite group with a U:P (or As) ratio of 3:2. It belongs to space group *Pca2*₁ and is a framework structure, consisting of uranyl arsenate sheets linked by uranyl pentagonal bipyramids. The uranyl arsenate sheets are based on the uranophane sheet–anion topology, which consists of alternating segments that are two uranyl arsenate chains wide and are highly corrugated rather than planar (12, 19). It has not been found to occur naturally (17).

Uranyl oxyhydroxide hydrates are extremely complex species, but their structures are all based on polyhedral sheets with the composition (UO₂)_x(O)_y(OH)_z, consisting of uranyl groups linked by oxide and hydroxide ions. Meta-schoepite is structurally related to naturally occurring schoepite, (UO₂)₄O(OH)₆·6H₂O, and they can be interconverted through exchange of water molecules in the structure, leaving the (UO₂)_x(O)_y(OH)_z sheets essentially unchanged in the process (20, 21). Meta-schoepite has 5 O_{eq} atoms distributed at 2.21–2.64 Å, and their backscattering is partially canceled out by each other. Therefore, the corresponding Fourier

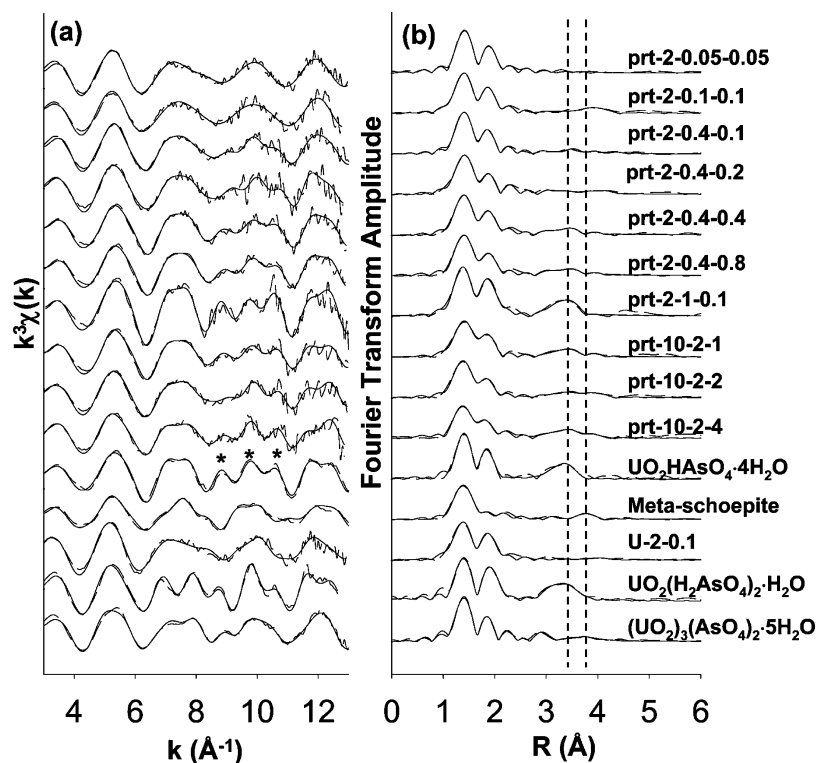


FIGURE 1. (a) k^3 -Weighted U L_{III} -edge EXAFS data of pretreated samples and model compounds. (b) Corresponding Fourier transforms in R space (not corrected for phase shift). U-2-0.1 is the sorption sample of U alone on untreated alumina. Raw data and shell-by-shell fitting results are shown by dashed and solid lines, respectively.

transform shows only a distribution of subtle weaker peaks after the first O_{ax} peak (Figure 1b). The O_{eq} can be fit with ~ 1.4 O at ~ 2.27 Å and ~ 1.7 O at ~ 2.44 Å. There are also 6 U atoms at 3.83 – 4.6 Å, which can be fit with ~ 2.1 U at ~ 3.87 Å and ~ 2.7 U at ~ 4.63 Å.

The U sorption sample on untreated alumina (U-2-0.1) shows a split equatorial shell with ~ 3.7 O_{eq} at ~ 2.34 Å and ~ 2.4 O at ~ 2.48 Å (Figure 1b), indicating the formation of an inner-sphere sorption complex (8, 9).

Arsenic K-edge EXAFS data of corresponding model compounds are shown in Figure 2, and their shell-by-shell fitting results are listed in Table SI-S2 of the Supporting Information. All samples can be fit with an As–O distance of ~ 1.68 Å, typical for AsO_4 tetrahedra. Overall, their As EXAFS χ curves show less striking differences as compared to those of the U EXAFS data, and similarities between $UO_2HAsO_4 \cdot 4H_2O$ and $UO_2(H_2AsO_4)_2 \cdot H_2O$ can again be observed, with U backscattering at ~ 3.7 Å. They differ in that $UO_2HAsO_4 \cdot 4H_2O$ has 4 U at ~ 3.7 Å, whereas $UO_2(H_2AsO_4)_2 \cdot H_2O$ has only 2 U atoms at this distance and also with As atoms at higher distances of ~ 4.3 and ~ 4.57 Å.

The As–alumina sorption sample (As-2-0.4) can be fit with 4 O atoms at ~ 1.68 Å and ~ 2 Al atoms at ~ 3.15 Å, indicating the formation of a bidentate inner-sphere surface sorption complex (22). On the basis of both EXAFS measurements and theoretical calculations, it is generally agreed that As(V) sorbs as a bidentate inner-sphere complex on various Al and Fe (hydr)oxides (22–24), although a monodentate surface complex has also been reported to exist at low surface coverage (25). The mechanism of phosphate adsorption on Al and Fe (hydr)oxides is under debate regarding different protonation states and bidentate vs monodentate complexes. However, by comparing calculated and experimental infrared spectroscopy results of phosphate surface sorption complexes, recent studies suggest that a bidentate bridging complex dominates at acidic pH range of 4–6, with various protonation states of monodentate surface complexes also becoming stable with increasing pH (26, 27). Therefore, the

analogy between arsenate and phosphate surface complexes for our experimental conditions is not unreasonable.

3.3. EXAFS Analysis of Sorption Products. As can be seen from Table 1, the pretreatment process clearly increased the amount of uranyl taken up by the alumina surface, to ~ 24 – 96% , as compared to only $\sim 23\%$ uptake without pretreatment (sample U-2-0.1). U L_{III} -edge EXAFS data for sorption samples and model compounds are shown in Figure 1a. The sequence, from top to bottom, corresponds to increasing alumina loading, $[As]_{ini}$, and $[U]_{ini}$. By simply comparing the shapes of the χ curves to those of the model compounds, it is seen that prt-2-0.05-0.05 is very similar to that of the U–alumina sorption sample, with a broad asymmetric peak at 6 – 9 Å $^{-1}$. With increasing As and/or U concentrations, this peak becomes narrower and more square, accompanied by the growth of a distinctive “triplet” feature at 9 – 10.5 Å $^{-1}$ (indicated by asterisks), very much like that for $UO_2HAsO_4 \cdot 4H_2O$ but dissimilar to the other U–As model compounds.

Figure 1b shows the corresponding Fourier transforms of sorption samples and model compounds. The two dominant peaks at 1 – 2 Å are typical of the uranyl moiety, with the first peak corresponding to the two axial oxygen atoms, O_{ax} , at distances typically of 1.77 – 1.83 Å (17) and the second peak corresponding to the equatorial oxygen atoms, O_{eq} . The number of equatorial oxygen atoms can range from 4 to 6 and, depending on the solution chemistry or solid structure, can either be at a relatively uniform distance or split into two or more shells at different distances. Burns (17) studied the bond length distribution of the equatorial shells in 222 structures containing the uranyl moiety and found the average lengths to be 2.264 , 2.368 , and 2.460 Å for structures with $O_{eq} = 4, 5,$ and 6 , with standard deviations of 0.064 , 0.01 , and 0.107 Å, respectively. All samples and model compounds also show a strong feature at ~ 3.2 Å, which is due to the 4-leg multiple scattering (MS) path composed of U–O–U with approximately 180° scattering between the central U atom and the two axial O atoms. All of the samples showing the

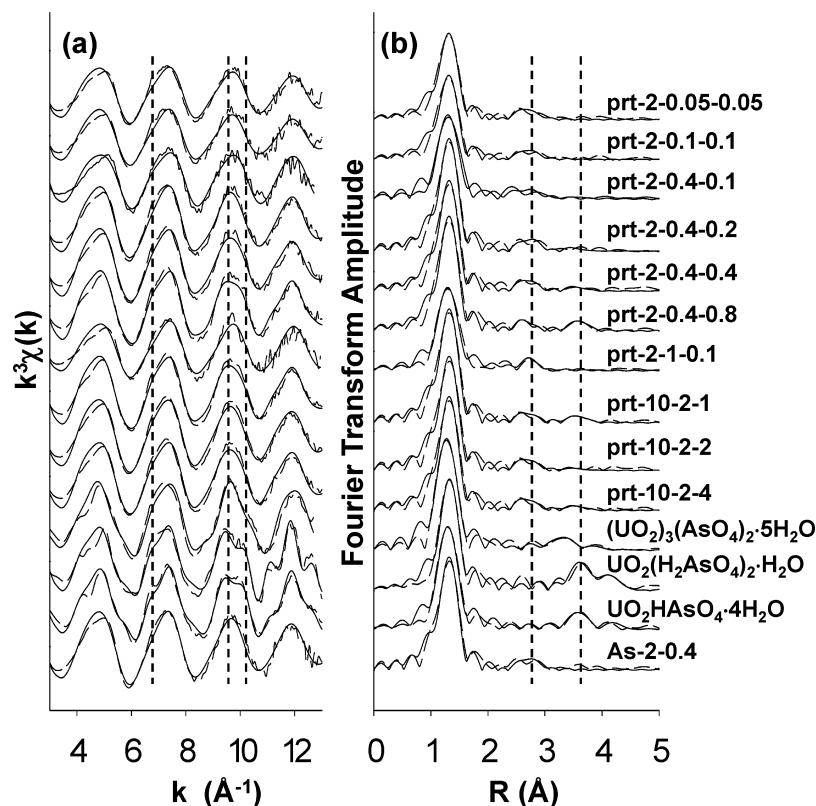


FIGURE 2. (a) k^3 -Weighted As K-edge EXAFS data of pretreatment samples and model compounds. (b) Corresponding Fourier transforms in R space (not corrected for phase shift). Raw data and shell-by-shell fitting results are shown by dashed and solid lines, respectively.

prominent triplet feature at $k = 9\text{--}10.5 \text{ \AA}^{-1}$ also show a strong feature at $\sim 3.2 \text{ \AA}$ in R space (indicated by dashed line), which is similar to that seen for $\text{UO}_2\text{HAsO}_4 \cdot 4\text{H}_2\text{O}$ and $\text{UO}_2(\text{H}_2\text{AsO}_4)_2 \cdot \text{H}_2\text{O}$. Samples in the high concentration group also show a weak peak at $\sim 4 \text{ \AA}$ (indicated by dashed line), similar to that of meta-schoepite, suggesting possible U polymeric species forming at high U concentrations.

Shell-by-shell fitting was carried out for all sorption samples, and the results are listed in Table 2. All of the samples can be fit with $\sim 2 \text{ O}_{\text{ax}}$ between 1.78 and 1.81 \AA , consistent with the $\text{O}=\text{U}=\text{O}$ moiety. The equatorial shell is best fit with a split O shell, with one at 2.28–2.35 \AA and another at 2.45–2.53 \AA , with the exceptions of prt-2-4-0.4, prt-2-4-0.8, and prt-2-1-0.1. These are best fit with only one equatorial oxygen shell ($\sim 4 \text{ O}$ atoms at $\sim 2.29 \text{ \AA}$) and are similar to those of model compounds $\text{UO}_2\text{HAsO}_4 \cdot 4\text{H}_2\text{O}$ and $\text{UO}_2(\text{H}_2\text{AsO}_4)_2 \cdot \text{H}_2\text{O}$. Arsenic backscattering at $\sim 3.7 \text{ \AA}$ is observed for all samples, suggesting the formation of a surface ternary complex and/or uranyl arsenate precipitates. A U–As path cannot be fit for the two lowest concentration series, prt-2-0.05-0.05 and prt-2-0.01-0.01, probably indicating that the surface-sorbed uranyl species are dominant in these samples. For samples of the high concentration group, U backscattering at 3.92–3.96 and 4.22–4.26 \AA are fit; these are typical U–U distances found for uranyl polymeric species or oxyhydroxide precipitates.

Arsenic K-edge EXAFS data are shown in Figure 2a. Fourier transforms of all of the sorption samples are dominated by a peak centered at $\sim 1.3 \text{ \AA}$, which is due to the backscattering of first oxygen shell and is best fit with $\sim 4 \text{ O}$ atoms at $\sim 1.69 \text{ \AA}$ (Table 3), which are typical values for As in tetrahedral coordination. Most of the sorption samples show a subtle shoulder at $\sim 6.7 \text{ \AA}^{-1}$ and a square-shaped peak at $8\text{--}10.5 \text{ \AA}^{-1}$ in k space (both indicated by dashed lines). These two features are similar to those in $\text{UO}_2\text{HAsO}_4 \cdot 4\text{H}_2\text{O}$ and $\text{UO}_2(\text{H}_2\text{AsO}_4)_2 \cdot \text{H}_2\text{O}$. However, a triplet feature can be seen for

$\text{UO}_2(\text{H}_2\text{AsO}_4)_2 \cdot \text{H}_2\text{O}$ at $10.5\text{--}13 \text{ \AA}^{-1}$ in k space, which is not observed in any of the sorption samples. Combining these observations with the U EXAFS results, we conclude that a phase similar to $\text{UO}_2\text{HAsO}_4 \cdot 4\text{H}_2\text{O}$ is more likely to be present in the sorption products than $\text{UO}_2(\text{H}_2\text{AsO}_4)_2 \cdot \text{H}_2\text{O}$. Figure 2b shows all of the sorption samples have a broad peak at $\sim 2.7 \text{ \AA}$ in R space (indicated by a dashed line), similar to that of the surface-sorbed As species. It can be fit with $\sim 2 \text{ Al}$ at $3.12 \pm 0.03 \text{ \AA}$ (Table 3), similar to that of the arsenate only sorption sample (i.e., As-2-0.4, fitting results in Table SI-S2 of the Supporting Information), suggesting that a bidentate inner-sphere sorption complex dominates on the surface. A few of the sorption samples, especially prt-2-0.4-0.8 and prt-10-2-1, show a prominent peak at $\sim 3.6 \text{ \AA}$ in R space (indicated by a dashed line), similar to the feature seen in $\text{UO}_2\text{HAsO}_4 \cdot 4\text{H}_2\text{O}$ and $\text{UO}_2(\text{H}_2\text{AsO}_4)_2 \cdot \text{H}_2\text{O}$, and can be fit with a U shell at $\sim 3.7 \text{ \AA}$ but generally with a very small coordination number. Attempts to fit this shell with an As–As correlation failed to yield satisfactory results.

One of the limitations of EXAFS is that the local structural information provided is averaged over all of the atoms of the particular element, thereby making it difficult to identify multiple species. However, based on the combined U and As EXAFS results, especially the distinctive splitting of the U(VI) equatorial oxygen shell for an inner-sphere surface sorption complex, As backscattering at 3.7 \AA for U–As precipitates, and U backscattering at 3.92–3.96 and 4.22–4.26 \AA for uranyl polymeric species, we hypothesize that the final sorption products most likely consist of multiple species. These include surface-sorbed uranyl (or arsenate) species, uranyl–arsenate precipitates (with a structure similar to that of trögerite), and polymeric uranyl species at high U concentrations ($\geq 2 \text{ mM}$). It is also possible that alumina–arsenate–uranyl ternary surface complexes exist in our system, especially at low U and As concentrations. However, identification of such complexes using EXAFS is difficult

TABLE 2. Fit Results of U L_{III}-Edge EXAFS Data on Sorption Samples

shell	CN ^a	R (Å)	σ ² (Å ²)	E ₀ (eV)	R ^b	shell	CN ^a	R (Å)	σ ² (Å ²)	E ₀ (eV)	R ^b
prt-2-0.05-0.05						prt-2-1-0.1					
O _{ax}	1.8	1.81	0.001	10.25	8.8	O _{ax}	2.7	1.78	0.003	5.48	8.3
O _{eq}	3.1	2.35	0.003 ^c			O _{eq}	4.3	2.29	0.002		
	2.1	2.50	0.003 ^c			As	3.6	3.70	0.005		
prt-2-0.1-0.1						prt-10-2-1					
O _{ax}	2 ^c	1.80	0.002	10.22	14.6	O _{ax}	2.5	1.8	0.005	11.64	8.9
O _{eq}	2.8	2.34	0.003 ^c			O _{eq}	3.2	2.31	0.003 ^c		
	2.3	2.51	0.003 ^c			As	1.2	2.47	0.003 ^c		
prt-2-0.4-0.1						prt-10-2-2					
O _{ax}	1.9	1.79	0.002	9.66	8.0	As	2.2	3.72	0.006 ^c		
O _{eq}	3.0	2.30	0.003 ^c			U	1.8	3.92	0.01 ^c		
	3.1	2.46	0.006			prt-10-2-2					
As	0.5	3.68	0.002			O _{ax}	2.1	1.79	0.003	7.94	8.0
prt-2-0.4-0.2						prt-10-2-2					
O _{ax}	2.6	1.81	0.004	13.62	9.0	O _{ax}	2.9	2.29	0.003 ^c		
O _{eq}	2.7	2.34	0.003 ^c			O _{eq}	2.0	2.45	0.003 ^c		
	1.8	2.53	0.003 ^c			As	0.7	3.70	0.002		
As	1.3	3.67	0.006 ^c			U	2.7	3.95	0.01 ^c		
prt-2-0.4-0.4						prt-10-2-4					
O _{ax}	1.8	1.78	0.001	10.72	6.8	O _{ax}	1.4	1.78	0.001	6.89	6.5
O _{eq}	4.3	2.29	0.005			O _{eq}	3.5	2.28	0.003 ^c		
As	1.1	3.68	0.003				2.8	2.45	0.003 ^c		
prt-2-0.4-0.8						prt-10-2-4					
O _{ax}	1.8	1.78	0.001	10.79	7.7	As	1.5	3.69	0.003		
O _{eq}	4.5	2.29	0.006			U	1.0	3.93	0.01		
As	1.2	3.68	0.003				0.7	4.28	0.006		

^a Coordination number. ^b Residual percent ^c Fixed.

TABLE 3. Fit Results of As K-Edge EXAFS Data of Sorption Samples

shell	CN ^a	R (Å)	σ ² (Å ²)	E ₀ (eV)	R ^b	shell	CN ^a	R (Å)	σ ² (Å ²)	E ₀ (eV)	R ^b
prt-2-0.05-0.05						prt-2-0.4-0.8					
O	3.2	1.69	0.002	4.85	19.6	O	4.3	1.69	0.002	5.55	17.6
Al	1.8	3.12	0.006 ^c			Al	1.4	3.11	0.006 ^c		
prt-2-0.1-0.1						prt-2-1-0.1					
O	3.3	1.69	0.003	5.01	20.1	U	0.5	3.71	0.001		
Al	1.6	3.13	0.006 ^c			prt-2-1-0.1					
prt-2-0.4-0.1						prt-10-2-1					
O	3.5	1.69	0.001	6.63	20.0	O	3.1	1.68	0.001	4.89	20.5
Al	2.2	3.09	0.006 ^c			Al	2.0	3.13	0.006 ^c		
prt-2-0.4-0.2						prt-10-2-1					
O	4.2	1.69	0.002	5.44	17.3	O	4.4	1.69	0.003	5.70	15.4
Al	2.0	3.15	0.006 ^c			Al	1.4	3.12	0.006 ^c		
prt-2-0.4-0.4						prt-10-2-2					
O	4.4	1.69	0.003	5.66	16.9	U	0.6	3.72	0.003		
Al	1.7	3.13	0.006 ^c			prt-10-2-2					
U	0.5	3.68	0.007			O	4.4	1.70	0.003	5.51	16.7
prt-2-0.4-0.8						prt-10-2-4					
O	4.4	1.69	0.003	5.66	16.9	Al	1.8	3.13	0.006 ^c		
Al	1.7	3.13	0.006 ^c			prt-10-2-4					
U	0.5	3.68	0.007			O	4.2	1.70	0.002	5.32	17.0
						Al	1.8	3.13	0.006 ^c		
						U	0.6	3.67	0.009		

^a Coordination number. ^b Residual percent. ^c Fixed.

because their corresponding interatomic distances using As or U as central atoms are likely to be similar to observations for systems containing both precipitation and surface adsorption, especially given the weak backscattering property of Al.

Principal component analysis (PCA) of U and As EXAFS data for sorption samples also suggests the existence of multiple species. Therefore, linear combination fits (LCF) were conducted to examine the relative percentage of each species. The selection and identification of end members are discussed in detail in the Supporting Information, and the results of LCF are shown in Table SI-S3 of the Supporting Information. LCF used U-alumina sorption sample (U-2-0.1), UO₂HAsO₄·4H₂O, and meta-schoepite as end members, representing a surface-sorbed uranyl species, uranyl-arsenate surface precipitates, and uranyl polymeric oxyhydroxide species. With increasing uranium concentration, the fraction

of surface-sorbed uranyl gradually decreases and the fraction of uranyl-arsenate precipitate increases. At high U concentrations (prt-10-2-2 and prt-10-2-4), uranyl polymeric species appear and increase with increasing U concentration. LCF results for As EXAFS suggest surface-sorbed As to be the dominant species in all sorption samples, and no obvious trend was observed with changes in concentrations.

3.4. X-ray Diffraction Evidence of Surface Precipitation.

XRD patterns of four representative sorption samples (prt-10-2-1, prt-2-1-0.1, prt-2-0.4-0.1, and prt-2-0.1-0.1) are shown in Figure 3. Data were collected using a Scintag diffractometer with a Cu Kα source and a Ge solid state detector at a scan rate of 0.3° 2θ/min. Also shown are the XRD patterns of γ-Al₂O₃ powder (unaged and untreated), UO₂HAsO₄·4H₂O, UO₂(H₂AsO₄)₂·H₂O, (UO₂)₃(AsO₄)₂·5H₂O, and meta-schoepite, with the intensities of the latter four

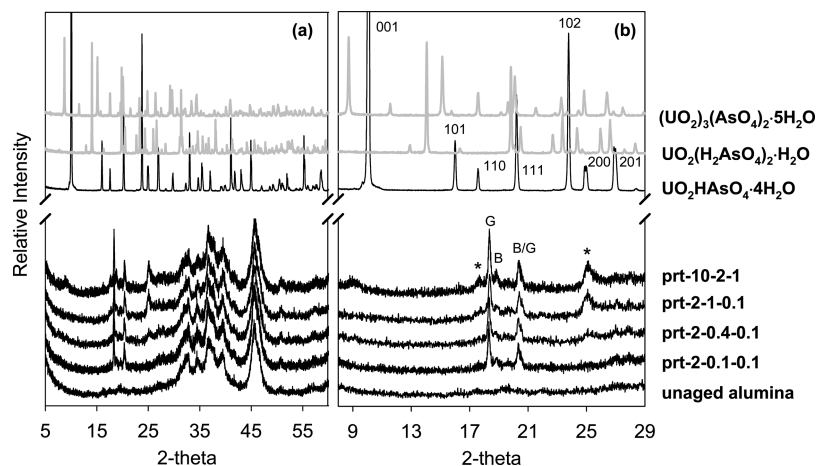


FIGURE 3. (a) XRD patterns of four representative pretreatment samples, prt-2-0.1-0.1, prt-2-0.4-0.1, prt-2-1-0.1, and prt-10-2-1 and model compounds. (b) Expanded view of (a) between 8° and 29° with the *hkl* of $\text{UO}_2(\text{H}_2\text{AsO}_4) \cdot 4\text{H}_2\text{O}$ indexed. B and G indicate peak positions corresponding to bayerite and gibbsite after the aging of γ -alumina. Asterisks indicate the peaks corresponding to surface precipitates in the sorption products.

scaled down to fit in Figure 3. As shown in Figure 3a, raw γ - Al_2O_3 shows broad, poorly defined maxima between 30° and 50° 2θ . The sharp peaks at ~ 18.5 , 19, and 20.5° 2θ in the aged samples (labeled G, B, and B/G in Figure 3b), respectively, correspond to bayerite and/or gibbsite. Two weak features at $\sim 18^\circ$ and 25° (indicated by asterisks) show gradual increases in intensity as pretreatment As concentration and alumina loading increase (from bottom to top), indicating the formation of surface precipitates. The EXAFS and LCF results suggested a progressive increase of a uranyl arsenate surface precipitate (with a structure similar to trögerite). These two peaks in the XRD pattern are consistent with trögerite but are not among its strongest diffraction peaks. This apparent inconsistency is probably due to structural features inherent to trögerite. As shown in Figure SI-S2 of the Supporting Information, the structure of trögerite consists of sheets containing uranyl bipyramids and arsenate tetrahedra. The interlayer region contains protons and H_2O molecules, and adjacent layers are linked through hydrogen bonding. This layered structure has been extensively studied and shows high proton conductivity and cation exchange between layers. Adding more complexity, the crystal structure can undergo a reversible phase transformation between high symmetry (tetragonal) and lower symmetry ($P\bar{1}$) structures near room temperature (18–28 °C) (16, 28). Therefore, depending on the crystallinity, ordering, and cation intercalation of the surface precipitates, some diffraction lines may have greatly attenuated intensity, especially the lines related to the repeat along the *c* axis. The two peaks that appear in Figure 3 at $\sim 18^\circ$ and 25° correspond to *110* and *200*, which are the two strongest peaks that do not have any *c* axis component. This evidence, combined with EXAFS results, which are more sensitive to short-range ordering of $<5 \text{ \AA}$ (here within a layer), suggests that the surface precipitate has a highly disordered, poorly crystalline structure similar to the sheets found in trögerite.

3.5. Environmental Implications. Combined with the results of our companion batch uptake study (7), we conclude that the pretreatment process is effective in enhancing uranyl sorption on alumina under acidic pH conditions as well as partially stabilizing the uranyl taken up by the surface. Multiple mechanisms are involved in U uptake, including surface adsorption and formation of uranyl arsenate surface precipitates and uranyl polymeric species or oxyhydroxides. The dominance of each mechanism depends on several factors such as sorbent particle loading, relative availability of surface sites, and most

importantly the absolute arsenate and uranyl concentrations and their ratio. The formation of a trögerite-like uranyl arsenate precipitate, as one of the dominant mechanisms suggests that U sequestered by this means is less likely to be released back into solution. These findings also demonstrate the importance of identifying the mechanisms for enhanced U uptake, which aids in evaluation of the long-term stability and potential remobilization of the sequestered U. Finally, the combined studies provide a conceptual basis for designing and evaluating pretreatment processes to enhance selective uptake of radionuclides. It is worth noting again that arsenate was chosen as an analog for phosphate, and this work therefore provides a starting point for assessment of phosphate, which might behave similarly. Although studies in more complex systems are needed, for example, the effects of pH and coexisting ligands (such as dissolved carbonate species) on uranyl sorption on pretreated surfaces, our work nevertheless provides predictive information regarding the final products in such systems.

Acknowledgments

This work was supported by the Center for Environmental Molecular Science at Stony Brook University through National Science Foundation Grant CHE-0221924. We thank beamline personnel at X11A (National Synchrotron Light Source) and 12-BM (Advanced Photon Source) for help with data collection, and L. Soderholm and S. Skanthakumar (Argonne National Laboratory) for assistance with sample handling and transportation through the Actinide Facility at Argonne National Laboratory. Use of the National Synchrotron Light Source and the Advanced Photon Source was supported by the U.S. Department of Energy, Office of Science, Office of Basic Energy Sciences, under Contracts DE-AC02-98CH10886 and DE-AC02-06CH11357, respectively. Comments from three anonymous reviewers and from Editor Dr. Ruben Kretzschmar greatly improved the manuscript.

Supporting Information Available

Descriptions of the synthesis methods for the three uranyl arsenate compounds and meta-schoepite, EXAFS data collection and analysis procedures, linear combination fitting methods and results, a figure of the structure of trögerite ($\text{UO}_2\text{HAsO}_4 \cdot 4\text{H}_2\text{O}$), tables of U L_{III} - and As K-edge EXAFS fitting results of model compounds, and LCF fits of U L_{III} - and As K-edge XAS data of sorption samples. This information

is available free of charge via the Internet at <http://pubs.acs.org>.

Literature Cited

- (1) Duff, M. C.; Coughlin, J. U.; Hunter, D. B. Uranium coprecipitation with iron oxide minerals. *Geochim. Cosmochim. Acta* **2002**, *66*, 3533–3547.
- (2) Fuller, C. C.; Bargar, J. R.; Davis, J. A.; Piana, M. J. Mechanisms of uranium interactions with hydroxyapatite: Implications for groundwater remediation. *Environ. Sci. Technol.* **2002**, *36*, 158–165.
- (3) Duff, M. C.; Hunter, D. B.; Hobbs, D. T.; Fink, S. D.; Dai, Z.; Bradley, J. P. Mechanisms of strontium and uranium removal from high-level radioactive waste simulant solutions by the sorbent monosodium titanate. *Environ. Sci. Technol.* **2004**, *38*, 5201–5207.
- (4) *Field Demonstration of Permeable Reactive Barriers to Remove Dissolved Uranium from Groundwater*; U.S. EPA Interim Report 402-C-00-001. U.S. Environmental Protection Agency: Fry Canyon, UT, 2000.
- (5) Liu, X. W.; Byrne, R. H. Rare earth and yttrium phosphate solubilities in aqueous solution. *Geochim. Cosmochim. Acta* **1997**, *61*, 1625–1633.
- (6) Fuller, C. C.; Bargar, J. R.; Davis, J. A. Molecular-scale characterization of uranium sorption by bone apatite materials for a permeable reactive barrier demonstration. *Environ. Sci. Technol.* **2003**, *37*, 4642–4649.
- (7) Tang, Y.; Reeder, R. J. Enhanced uranium sorption on aluminum oxide pretreated with arsenate. Part I: Batch uptake behavior. *Environ. Sci. Technol.* **2009**, DOI: 10.1021/es802369m.
- (8) Sylwester, E. R.; Hudson, E. A.; Allen, P. G. The structure of uranium(VI) sorption complexes on silica, alumina, and montmorillonite. *Geochim. Cosmochim. Acta* **2000**, *64*, 2431–2438.
- (9) Froideval, A.; Nero, M. D.; Gaillard, C.; Barillon, R.; Rossini, I.; Hazemann, J. L. Uranyl sorption species at low coverage on Al-hydroxide: TRIFS and XAFS studies. *Geochim. Cosmochim. Acta* **2006**, *70*, 5270–5284.
- (10) Kowal-Fouchard, A.; Drot, R.; Simoni, E.; Ehrhardt, J. J. Use of spectroscopic techniques for uranium(VI)/montmorillonite interaction modeling. *Environ. Sci. Technol.* **2004**, *38*, 1399–1407.
- (11) Baumann, N.; Brendler, V.; Arnold, T.; Geipel, G.; Bernard, G. Uranyl sorption onto gibbsite studied by time-resolved laser-induced fluorescence spectroscopy (TRLFS). *J. Colloid Interface Sci.* **2005**, *290*, 318–324.
- (12) Finch, R.; Burns, P. C., Eds. Systematics and Paragenesis of Uranium Minerals. In *Uranium: Mineralogy, Geochemistry, and the Environment*; Mineralogical Society of America: Chantilly, VA, 1999; Vol. 38, pp 124–132.
- (13) Parkhurst, D. L.; Appelo, C. A. J. *User's Guide to PHREEQC: A Computer Program for Speciation, Batch Reaction, One-Dimensional Transport, and Inverse Geochemical Calculations*, version 2; U. S. Geological Survey, Water Resources Investigations Report 99-4259: Denver, CO, 1999; p 310.
- (14) Sandino, A.; Bruno, J. The solubility of $(\text{UO}_2)_3(\text{PO}_4)_2 \cdot 4\text{H}_2\text{O}$ and the formation of U(VI) phosphate complexes: Their influence in uranium speciation in natural waters. *Geochim. Cosmochim. Acta* **1992**, *56*, 4135–4145.
- (15) Vesely, V.; Pekarek, V.; Abbrent, M. A study on uranyl phosphates. III. Solubility products of uranyl hydrogen phosphate, uranyl orthophosphate, and some alkali uranyl phosphates. *J. Inorg. Nucl. Chem.* **1965**, *27*, 1159–1166.
- (16) Locock, A. J.; Burns, P. C.; Duke, M. J. M.; Flynn, T. M. Monovalent cations in structures of the meta-autunite group. *Can. Mineral.* **2004**, *42*, 973–996.
- (17) Burns, P. C. U^{6+} minerals and inorganic compounds: Insight into an expanded structural hierarchy of crystal structures. *Can. Mineral.* **2005**, *43*, 1839–1894.
- (18) Gelsing, T. M.; Ruscher, C. H. Structure and properties of $\text{UO}_2(\text{H}_2\text{AsO}_4)_2 \cdot \text{H}_2\text{O}$. *Z. Anorg. Allg. Chem.* **2000**, *626*, 1414–1420.
- (19) Locock, A. J.; Burns, P. C. Structures and syntheses of framework triuranyl diarsenate hydrates. *J. Solid State Chem.* **2003**, *176*, 18–26.
- (20) Finch, R. J.; Hawthorne, F. C.; Ewing, R. C. Structural relations among schoepite, metaschoepite and “dehydrated schoepite”. *Can. Mineral.* **1998**, *36*, 831–845.
- (21) Weller, M. T.; Light, M. E.; Gelbrich, T. Structure of uranium(VI) oxide dihydrate, $\text{UO}_3 \cdot 2\text{H}_2\text{O}$; synthetic meta-schoepite $(\text{UO}_2)_4\text{O}(\text{OH})_6 \cdot 5\text{H}_2\text{O}$. *Acta Crystallogr., Sect. B: Struct. Commun.* **2000**, *56*, 577–583.
- (22) Arai, Y.; Elzinga, E. J.; Sparks, D. L. X-ray absorption spectroscopic investigation of arsenate and arsenite adsorption at the aluminum oxide–water interface. *J. Colloid Interface Sci.* **2001**, *235*, 80–88.
- (23) Waychunas, G. A.; Rea, B. A.; Fuller, C. C.; Davis, J. A. Surface chemistry of ferrihydrite. 1. EXAFS studies of the geometry of coprecipitated and adsorbed arsenate. *Geochim. Cosmochim. Acta* **1993**, *57*, 2251–2269.
- (24) Sherman, D. M.; Randall, S. R. Surface complexation of arsenic(V) to iron(III) (hydr)oxides: Structural mechanism from ab initio molecular geometries and EXAFS spectroscopy. *Geochim. Cosmochim. Acta* **2003**, *67*, 4223–4230.
- (25) Fendorf, S.; Eick, M. J.; Grossl, P.; Sparks, D. L. Arsenate and chromate retention mechanisms on goethite. 1. Surface structure. *Environ. Sci. Technol.* **1997**, *31*, 315–320.
- (26) Kubicki, J. D.; Kwon, K. D.; Paul, K. W.; Sparks, D. L. Surface complex structures modelled with quantum chemical calculations: carbonate, phosphate, sulphate, arsenate, and arsenite. *Eur. J. Soil Sci.* **2007**, *58*, 932–944.
- (27) Kwon, K. D.; Kubicki, J. D. Molecular orbital theory study on surface complex structures of phosphates to iron hydroxides: Calculation of vibrational frequencies and adsorption energies. *Langmuir* **2004**, *20*, 9249–9254.
- (28) Fitch, A. N.; Fender, B. E. F.; Wright, A. F. The structure of deuterated lithium uranyl arsenate tetrahydrate $\text{LiUO}_2\text{AsO}_4 \cdot 4\text{D}_2\text{O}$ by powder neutron diffraction. *Acta Crystallogr., Sect. B: Struct. Commun.* **1982**, *38*, 1108–1112.

ES802370D